energies

MDPI

Article

Deeper Understanding of Ternary Eutectic Carbonates/Ceria-Based Oxide Composite Electrolyte through Thermal Cycling

André Grishin [1,2], Manel Ben Osman [1], Haïtam Meskine [1], Valérie Albin [1], Virginie Lair [1], Michel Cassir [1] and Armelle Ringuedé [1,*]

[1] Chimie ParisTech, CNRS, Institut de Recherche de Chimie Paris, PSL University, 11 Rue Pierre et Marie Curie, 75005 Paris, France; andre.grishin@totalenergies.com (A.G.); benosman.manel@gmail.com (M.B.O.); haitam.meskine@gmail.com (H.M.); valerie.albin@chimieparistech.psl.eu (V.A.); virginie.lair@chimieparistech.psl.eu (V.L.); michel.cassir@chimieparistech.psl.eu (M.C.)

[2] TotalEnergies One Tech, 2 Place Jean Millier, 92400 Courbevoie, France

* Correspondence: armelle.ringuede@chimieparistech.psl.eu; Tel.: +330-185-784-203

Abstract: Due to a high conductivity of about 0.1 S·cm^{-1}, Li-Na-K carbonate eutectic and Sm-doped ceria composite material is a good electrolyte candidate for hybrid fuel cells operating between 500 °C and 600 °C. The present paper aims at a deeper understanding of the species and mechanisms involved in the ionic transport through impedance spectroscopy and thermal analyses, in oxidizing and reducing atmospheres, wet and dry, and during two heating/cooling cycles. Complementary structural analyses of post-mortem phases allowed us to evidence the irreversible partial transformation of molten carbonates into hydrogenated species, when water and/or hydrogen are added in the surrounding atmospheres. Furthermore, this modification was avoided by adding CO_2 in anodic and/or cathodic compartments. Finally, a mechanistic model of such composite electrical behavior is suggested, according to the surrounding atmospheres used. It leads to the conclusions that cells based on this kind of electrolyte would preferably operate in molten carbonate fuel cell conditions, than in solid oxide fuel cell conditions, and confirms the name of "Hybrid Fuel Cells" instead of Intermediate Temperature (or even Low Temperature) Solid Oxide Fuel Cells.

Keywords: carbonate eutectic/ceria composite; multi-ionic conductor; SOFC; MCFC; hybrid fuel cell electrolyte; transport mechanisms; thermal cycling

Citation: Grishin, A.; Ben Osman, M.; Meskine, H.; Albin, V.; Lair, V.; Cassir, M.; Ringuedé, A. Deeper Understanding of Ternary Eutectic Carbonates/Ceria-Based Oxide Composite Electrolyte through Thermal Cycling. *Energies* **2022**, *15*, 2688. https://doi.org/10.3390/en15072688

Academic Editor: Stephen McPhail

Received: 25 January 2022
Accepted: 16 March 2022
Published: 6 April 2022

1. Introduction

Composite materials based on molten salts and solid oxide phase has been suggested by Zhu and Mellander since the 1990s, highlighting high protonic conductivities in the 300–600 °C temperature range. These materials combined oxoacid salt and alumina [1]. This concept has been next widely studied, varying both the molten salts and the solid oxide phase. Rapidly, the use of doped-ceria has been outlined, as yttria-stabilized zirconia (YSZ) was not stable in such combinations [2]. Thus yttria-doped ceria (YDC), samaria-doped ceria (SDC) and gadolinia-doped ceria (GDC), and even co-doped ceria [3–8] have been associated with chlorides [9–14], hydroxides [15], carbonates [16] and also with sulfates [17–19]. Most of the literature has recently been dedicated to molten carbonates and ceria-based oxide composites. The high level of conductivity (>0.1 S·cm^{-1}) is more than 10 to 10^3 times the GDC and YSZ single phase conductivities at 600 °C, respectively. Moreover, single cells based on these composites as electrolytes can reach performances up to 1 to 2 W·cm^{-2} in terms of power density in the 500–600 °C temperature range [15,20–29].

It is worth mentioning that the composite material suggested by Zhu et al. [15] is close to the usual electrolyte structure of Molten Carbonate Fuel Cells (MCFC) electrolyte, composed of a lithium aluminate ($LiAlO_2$) porous matrix embedding molten carbonates, and operating close to 600 °C. For this reason, usual binary eutectic compositions,

such as $(Li_{0.52}Na_{0.48})_2CO_3$ and $(Li_{0.62}K_{0.38})_2CO_3$ are associated with the solid oxide phase in a composite electrolyte. The difference is that the porous $LiAlO_2$ matrix is electrically insulating in MCFC, whereas it is replaced by an ionic conductive material in the molten carbonates/ceria-based composite. Surprisingly, such cells based on molten carbonate/ceria were called "Intermediate Temperature Solid Oxide Fuel Cells", which apparently is not fully correct.

Despite the fact that their high power densities are reached in a lower temperature range than the operating temperature of classical Solid Oxide Fuel Cells (SOFC), and are largely higher than for MCFC at 600 °C (a factor of 5 to 10) [30], the development of fuel cells based on composite electrolyte suffers from a lack of data on medium or long-term performances. Li and Sun [31] reported that for a SDC-$(Li,Na)CO_3$ composite based single cell, open circuit potential (OCP) was relatively stable despite some small losses in power densities, even after 200 h of operation at 650 °C in MCFC atmosphere conditions, thus, by using CO_2-based atmospheres on both the anode and cathode compartments.

Benamira et al. has shown that the electrolyte could be relatively stable in terms of conductivity during 6000 h in air [32]. In the same reference, it was also clearly shown that depending on the surrounding atmosphere considered, in single and dual atmospheres electrochemical tests, the electrical behavior was hugely different, and this could finally be a problem for a long-term single cell operation.

Then, Benamira et al. completed their study with electrochemical tests, varying the ceria particle size. It was shown that single cell performances were increased by the use of nanoparticles. This was consistent with the assumptions of several groups, assuming that molten carbonates/solid oxide phase interfaces, acting as "super ionic pathways", were at the origin of the conductivity enhancement; and by increasing the length of interface, the conductivity and the performances were also increased [16,17,33,34]. J. Maier justified this with the formation of a space charge layer at the interface, by an accumulation of oxide ions at the interface, as well as the metallic cations from the carbonate side [35]. It is also worth mentioning the theoretical calculations from Ricca et al., performed to better understand interface reactivity in composites based on binary carbonate eutectics YSZ-$(Li,K)_2CO_3$ and TiO_2-$(Li,K)_2CO_3$ [2,36–40].

Numerous authors working on the composites agreed with the multi-ionic conductor specificity of these materials [41]. In the last few years, some schemes resuming the species involved [42], clearly showed an evolution from the first suggested mechanisms by Zhu et al., restricted initially to two percolating phases involving both oxide ions and protons in oxide phase and molten carbonate, respectively [15]. At a minimum, all ions involved in cerium oxide phase usual transport (oxygen vacancies) and molten carbonate phase (alkaline metal cations and carbonate ions) contribute to the total behavior. Some protons are also mentioned in the theoretical approach [34], as claimed initially by Bin Zhu, although this is a hugely controversy subject. Protons cannot exist as "free protons" in such phases, however, some hydrocarbonates or even hydroxide ions could be considered.

In the present paper, we are interested in studying ternary eutectic carbonate composition $(Li,Na,K)_2CO_3$ associated with samaria-doped ceria (SDC). The first reason is the lower melting temperature compared to binary (Li,K)- or (Li,Na)-carbonate eutectics. Furthermore, when associated with SDC instead of gadolinia-doped ceria (GDC), single cells performances were higher: 720 $mW{\cdot}cm^{-2}$ at 650 °C and 224 $mW{\cdot}cm^{-2}$ at 600 °C as first reported in the literature by Xia et al. [43]. It is important to note that CO_2 was present in cathodic atmosphere [20]. After optimization of the powder synthesis, they reached a power density of 1.1 $W{\cdot}cm^{-2}$ at 550 °C, and an electrolyte conductivity of 0.4 $S{\cdot}cm^{-1}$ [6]. Thus, we studied the electrical behavior of SDC-$(Li,Na,K)_2CO_3$ composite electrolyte as a function of temperature, atmosphere compositions (reducing and oxidizing, dry or wet, with CO_2 addition or not) and during two heating/cooling cycles in order to implement the knowledge about transport mechanisms and species involved in the total conductivity. This was performed through impedance spectroscopy measurements, combined with Dif-

ferential Scanning Calorimetry (DSC) analysis, *post-mortem* X-ray diffraction experiments and microscopic observations.

2. Materials and Methods

2.1. Preparation of Sm-Doped Ceria-(Li,Na,K)$_2CO_3$ Composite Electrolyte

The composite electrolyte was prepared by the solid–solid method according to the previously described procedure [32,44]. First, a ternary eutectic mixture of Li_2CO_3-Na_2CO_3-K_2CO_3 (43.5-31-5-25.0) %mol., (noted hereinafter as LiNaK), was prepared by mixing commercial salt powders (purity $\geq$ 99.8%, *Sigma Aldrich*, Saint Quentin Fallavier 38297, France) in stoichiometric amount. The mixture was well ground, heated up to 650 °C (3 °C·min^{-1}) and maintained at this temperature for 1 h under dry 30 %vol. CO_2 in synthetic air (*Air Liquide*, 75 Quai d'Orsay, Paris 75007, France). After cooling (3 °C·min^{-1}), the eutectic mixture was carefully ground to attain the state of a fine powder. The second step was the mixing of as-prepared eutectic to a commercially available samaria-doped ceria (SDC) powder $Ce_{0.8}Sm_{0.2}O_{1.9}$ (purity $\geq$ 99.9%, *Fuel Cell Materials*, 404 Enterprise Dr, Lewis Center, OH 43035, USA) in proportion of 30–70 %wt. for SDC-LiNaK. Ground composite mixture was thermally treated under the same conditions as the eutectic, with one difference: the cooling was replaced by a quenching to room temperature; then the mixture was ground thoroughly again. All grinding operations during the composite synthesis were performed in a porcelain mortar.

Electrolyte pellets were made from the oxide-carbonate composite powder, by a dry press technique. Placed in a 13-mm-diameter mold, 0.9 g of powder was pressed by uniaxial pressure equivalent to 4 t applied for 5 min. Then, the pellets were sintered in air at 600 °C for 1 h, with a rate of 5 °C·min^{-1} for both heating and cooling steps. All as-prepared pellets were kept in an oven at 120 °C before and after electrochemical tests.

2.2. Electrochemical Analysis

Electrical behavior of SDC-LiNaK electrolyte was carried out by electrochemical impedance spectroscopy (EIS) using a two-electrode symmetric configuration [44]. Electrodes were formed as follows: M-0034 gold paste (*Metalor*, 74 Warstone Lane, Birmingham, UK) was deposited on both parallel faces of the pellet, heat-treated next for 1 h at 600 °C in air (heating and cooling rates were 1 °C·min^{-1}), ensuring as-made electrodes' electrical resistance was lower than 1 Ohm.

To perform the conductivity measurements, the sample was introduced in Open-Flanges™ fuel cell test bench (*Fiaxell*, Lausanne, Switzerland), allowing to work in single or dual controlled atmospheres. Gold wires connected to gold meshes were used as current collectors on both sides of the pellet. The electrical behavior of such symmetrical half-cells was studied under synthetic air, nitrogen, hydrogen/nitrogen mixtures, with or without carbon dioxide, dry or wet atmospheres. Test conditions in terms of atmospheric compositions are displayed in Table 1. All high purity grade gases ($\geq$99.999%) were supplied by *Air Liquide* (75 Quai d'Orsay, Paris 75007, France). Dry hydrogen of the same purity was produced from deionized water ($\geq$18.2 MOhm·cm) by the laboratory HK-250 generator (*LNI Schmidlin*, Versoix, Switzerland). The resulting gas flow rate through the cell was 150 cm^3·min^{-1}, whatever the atmosphere used. When required, a constant vapor flow was generated by an integrated steamer (*Fiaxell*, Lausanne, Switzerland) from the same quality water inside the test bench.

Impedance spectroscopy measurements were performed using a Modulab Solartron Analytical potentiostat (Princeton Applied Research, 1100 Cassatt Road Berwyn, PA 19312, USA) with a FRA 1MHz frequency analyzer module, in a 10 MHz–0.1 Hz frequency range (11 points per decade), applying a 100 mV-amplitude alternative voltage signal, with respect to the system linear behavior. Between each measurement, once the desired temperature had been reached, a minimum hold of 15 min had been observed for the thermal stabilization of the sample. Data were collected by XM-Studio ESC software (Princeton Applied Research, 1100 Cassatt Road Berwyn, PA 19312, USA).

Table 1. Composition and corresponding Arrhenius plots of gaseous mixtures during EIS thermal cycling analysis.

Atmosphere	Gas Mixture	Composition (vol.%)	Corresponding Arrhenius Plot
Reference	N_2	100	Figures 1a and 4
Dry oxidizing	N_2/O_2	80/20	Figure 1b
Wet oxidizing	$N_2/O_2/H_2O$	(80/20) hum. 20%	Figure 6a
Dry reducing	N_2/H_2	77/23 50/50 0/100	Figures 2–4 Figure 4
Wet reducing	$N_2/H_2/H_2O$	(77/23) hum. 20%	Figure 6b
MCFC oxidizing	$N_2/O_2/CO_2$	56/14/30	Figure 7a
MCFC reducing	$H_2/CO_2/H_2O$	64/16/20	Figure 7b

2.3. Phase and Microstructural Analysis

Phase composition of SDC-LiNaK composite electrolyte was determined before and after electrochemical tests by X-Ray diffraction using Bragg–Brentano geometry. All samples were analyzed as pellets. The irradiated surface was prepared by removing metallic electrode and then manually polishing on 2000-grit SiC sand disc to ensure a good flatness. The as-synthesized pellet was only polished on one side after synthesis. Measurements were performed on a D8 Endeavor diffractometer (*Bruker*, Billerica, MA, USA) equipped with a Co anticathode ($\lambda_{K_\alpha 1}$ = 1.78897 Å, $\lambda_{K_\alpha 1}$ = 1.79285 Å, $\lambda_{K_\alpha 1}/\ \lambda_{K_\alpha 2}$ = 0.5) operated at 35 kV and 28 mA and an energy dispersive Lynxeye (*Bruker* Billerica, MA, USA) detector with integrated K_β filtering. Data was collected from 20 to 100°2θ, with a step of 0.0257°2θ within 15 s. The sample holder rotation rate was kept at 10 rpm. The phase components were identified using the HighScore (*PanAlytical*, Almelo 7602 EA, The Netherlands) software and the PDF-4+ RDB database purchased by ICDD (International Center for Diffraction Data).

2.4. Thermal Analysis

Simultaneous Thermogravimetric and Differential Scanning Calorimetry analysis (TGA-DSC) were performed on Setsys Evolution ATG 16/18 easy fit analyzer (*Setaram*, Caluire et Cuire 69300, France). The powder electrolyte samples were placed in the alumina 100 µL crucibles so as to fill the crucible to $\frac{3}{4}$ full. The same empty crucible was used as reference during acquisition of DSC signal by an S-type sensor (Pt/PtRh 10%, *Setaram*, Caluire et Cuire 69300, France). The temperature scanning rate was 2 °C·min^{-1} during heating and cooling stages, all performed in the 40–600 °C range under atmospheric pressure and 50 cm^3·min^{-1} gas flow rate. High purity argon (≥99.999%, *Air Liquide*, 75 Quai d'Orsay, Paris 75007, France) was used as an inert gas for analysis, and also as a base to form different percentage hydrogen mixtures. A dry hydrogen (≥99.999% of purity) was produced by the HK-250 generator (*LNI Schmidlin*, Versoix, Switzerland). Data were collected and processed using Calisto software (*Setaram*, Caluire et Cuire 69300, France).

3. Results and Discussion

Whatever the gaseous atmospheric composition, the composite impedance was measured at different temperatures, during two heating and cooling cycles. As reported in Figure 1, the conductivity does not follow a single Arrhenius law in all the temperature range explored, i.e., from 200 and 650 °C typically. A peculiar sigmoid shape described the composite electrical behavior, as already mentioned by several groups from the first studies dealing with these families of composites as fuel cell electrolytes [12,32,44–48]. Indeed, three regions can be distinguished during the first heating, with two Arrhenius behaviors at low temperature (noted LT, below 360 °C) and high temperature (noted HT, higher

than 400 °C), with activation energies equal to 2.0 eV and 0.27 eV, respectively, in nitrogen (Figure 1a). It is worth noting that the activation energy calculated at low temperature when 20% of oxygen is added (Figure 1b) is half of what is determined in pure nitrogen, indicating the probable impact of oxide ions contribution to the total conductivity, limited in nitrogen atmosphere. However, no modification is observed at the highest temperature range explored and is ascribed to the molten carbonate contribution embedded in the solid oxide phase. The usual activation energy of ternary carbonate eutectic when the conductivity is measured from a molten bath is, however, slightly higher, between 0.26 eV and 0.42 eV, referring to Lair et al. [49] and Ward and Janz [50].

These two regions on Arrhenius plots are separated by a narrow region (called transition region) in terms of temperature (30 to 40 degrees), ending close to the melting temperature of the ternary carbonate eutectic mixture (397 °C) [51] as will be seen later by DSC measurements in the same atmosphere, yielding to a huge gain of a factor 10^3 to 10^4 in the conductivity from low to high levels. This transition zone corresponds, whatever the molten salt considered, to the salt mixture progressive melting process. The interface between the molten carbonate phase and the solid oxide phase SDC is considered to be important in relation to this transition region. Indeed, a large number of authors adopted one model, consisting of H^+ or HCO_3^- migration at the interface solid oxide/carbonate, thus promoting the conduction mechanism in the vicinity of the interface [15,17,34,43]. However, as the present results were obtained in dry air, no hydrogen (whatever its form) was present in the surrounding atmosphere, and thus, this model makes no real sense. According to Maier et al. [35], a space charge zone is formed at the interface between both conductive phases, with an increase in oxide ions vacancies concentrations compared to the volume content. This phenomenon, which is more realistic, is more pronounced as far as the temperature increases up to the ternary eutectic melting temperature, yielding to the molten carbonate percolation as the carbonate phase would be continuous in our case, with more than 30 %wt [52,53].

As in our previous studies, SDC-LiNaK composite electrical behavior was revealed in a nitrogen atmosphere in order to guarantee a reference-kind behavior. The conductivity variation as a function of the reverse temperature was as expected, with the previous described evolution, following three temperature regions. More interesting was the stable electrical behavior during two heating/cooling cycles. No change was observed as reported in Figure 1a,b, in N_2 and synthetic dry air, respectively.

Considering the electrical behavior in hydrogen-containing atmospheres, it is really quite different to that shown in Figures 2–4. One can note that there are still three regions during the first heating corresponding to the similar temperature ranges as described before in nitrogen and dry air. First, we observe that the end of the transition zone is slightly higher, 406 °C instead of 397 °C. Moreover, at higher temperatures, the activation energy decreased down to 0.21 eV. This could be justified by the appearance of a part of electronic conduction following doped ceria reduction in hydrogen, according to the simplified Reaction (1). This reduction reaction can be rewritten as Reaction (2), taking into account the defect chemistry, according to the Kröger–Vink notation:

$$2CeO_2 + H_2 \rightarrow Ce_2O_3 + H_2O \quad (1)$$

$$H_{2(g)} + O_O^{\times} \rightarrow V_O^{\bullet\bullet} + 2e' + 2H_2O \quad (2)$$

where $O_O^{\times}$ is an oxygen in its regular position in ceria lattice and $V_O^{\bullet\bullet}$ is an oxygen vacancy, e' is an electronic defect negatively charged, as an electron.

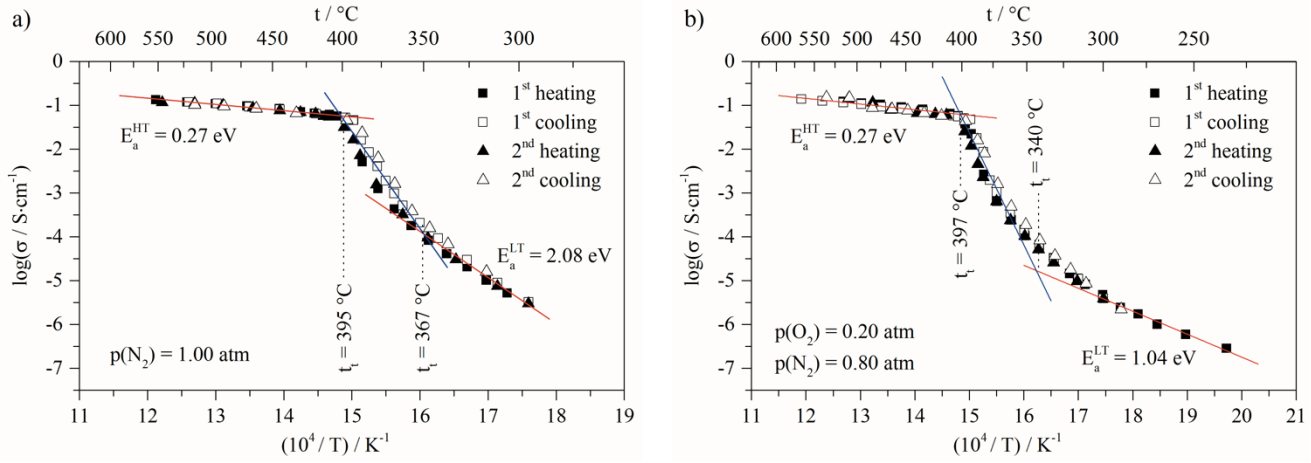

Figure 1. Arrhenius diagrams of the conductivity during two heating/cooling cycles for SDC—LiNaK composite electrolyte performed under pure nitrogen (**a**) and synthetic dry air (**b**) atmospheres. Activation energy values were obtained within low (E_a^{LT}) and high (E_a^{HT}) temperature regions of diagrams. Transition temperatures are defined by t_t.

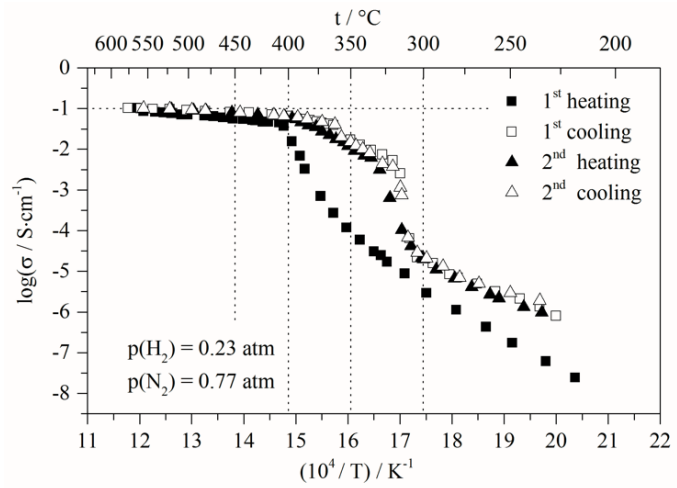

Figure 2. Arrhenius diagram of the conductivity during two heating/cooling cycles for SDC—LiNaK composite electrolyte performed under 23%—H_2—in—N_2 dry atmosphere.

The second point is that the composite electrical behavior drastically changed during the first cooling. Not only one but two drops in conductivity are now observed, as well as some changes in the slope values. This kind of evolution has already been pointed out in a previous work dealing with binary carbonate eutectic combined with Gd-doped ceria [2]. A partial transformation of molten carbonates into molten hydroxide-containing mixture was suggested, due to the associated recrystallization of LiOH- or NaOH-carbonate-based mixtures, close to 360 and 310 °C, respectively. Nevertheless, the most important result is that the electrical behavior of the composite seems to be stabilized during the second heating/cooling cycle as the transition temperatures remain the same as during the first cooling.

Moreover, by increasing the amount of hydrogen in the surrounding atmosphere, the level of conductivity is increased, which is clearly highlighted at intermediate and low temperature ranges. It is worth mentioning that the activation energy values, corresponding to the three new linear regions observed during cooling, are modified as shown in Figure 3:

- At low temperature (<307 °C), before the first transition, the activation energy decreased from 1.58 eV to 1.02 eV, related to the first heating and cooling steps, respectively;
- At high temperature (>410 °C) the activation energy decreased from 0.21 eV to 0.12 eV. This variation clearly indicates that the transport mechanisms and/or the species

involved are modified. Moreover, the next change of slope is observed at around 406 °C down to 361 °C, and the activation value is 0.49 eV (Figure 3b). This value is close to the isolated molten ternary eutectic as reported by Ward et al. [50]. However, this should have been the same value of up to 490 °C, as in his work, which was not the case in our study; as this temperature is included in the temperature range, for which the activation is lower, being 0.12 eV. The other assumption is that this activation energy value of 0.49 eV quite often corresponds to protonic conduction through hydroxide ions [54–56]. The following slope, around 360–315 °C temperature range, is close to 1.2 eV, and is not fully identified. Nevertheless, assuming the partial transformation of carbonates into hydroxides, this could be ascribed to hydroxide transport mixed with carbonates into the porous solid matrix. The activation energy values corresponding to the different regions of the Arrhenius plots present in this paper are calculated in the same way, and can be found in the Supplementary Information.

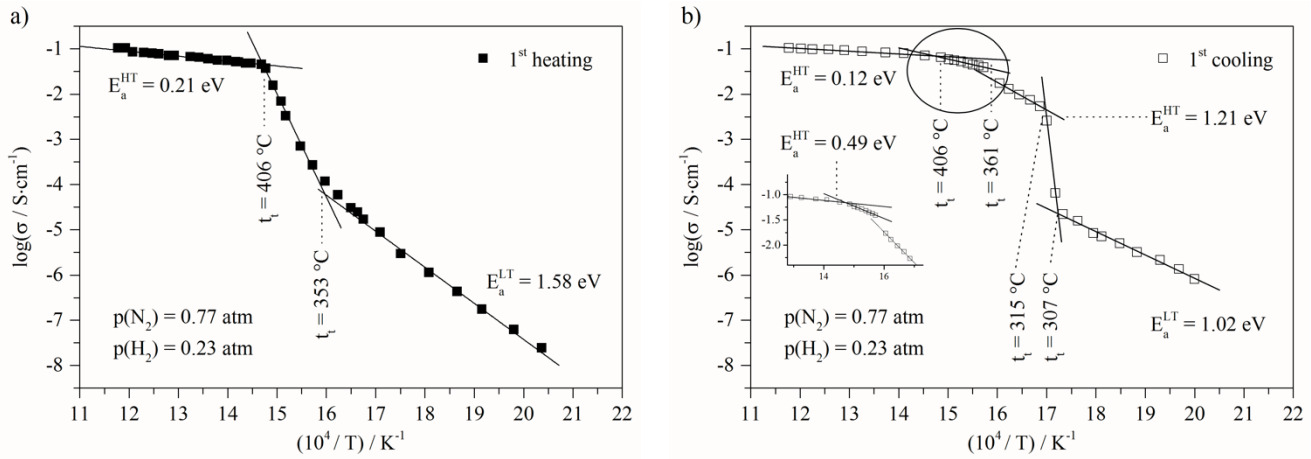

Figure 3. Focus on the first cycle: two Arrhenius diagrams in dry 23%—H_2—in—N_2 for SDC—LiNaK composite electrolyte: (**a**) heating and (**b**) cooling. Activation energy values were obtained within low (E_a^{LT}) and high (E_a^{HT}) temperature regions of diagrams. Transition temperatures are defined by t_t.

Thus, one may assume that the hydrogen oxidation in carbonate media can yield to the transformation of carbonate ions into hydroxides, according to Reaction (3). That also means that CO_2 is locally formed and, consequently, it avoids a more or less deep decarbonation of the carbonate media and transformation of carbonates into alkali oxides. Furthermore, this phenomenon can be described by Reaction (4), considering the defect chemistry, fully involving defects originated at the interface, regarding oxygen vacancies from ceria phase side and hydrocarbonate and hydroxide ions formation on the carbonate phase side:

$$H_{2(g)} + 2CO_3^{2-} \leftrightarrow 2CO_2 + 2OH^- + 2\bar{e} \quad (3)$$

$$H_{2(g)} + V_O^{\bullet\bullet} + O_O^{\times} + (CO_3)_{CO_3}^{\times} \leftrightarrow (OH)_O^{\bullet} + (HCO_3)_{CO_3}^{\bullet} \quad (4)$$

where $(OH)_O^{\bullet}$ is hydroxyl ion occupying an oxygen regular site in cerium oxide phase and $(HCO_3)_{CO_3}^{\bullet}$ represents the formation of hydrocarbonate occupying a carbonate position in the melt.

This last mechanism (Reaction (4)) has been suggested by Xiong et al. [57] studying composite based on yttrium-doped barium zirconate (BZY) associated with binary $(Li,Na)_2CO_3$ carbonate eutectic. In the case of SDC-LiNaK, as cation defect concentration is elevated at the interface, one can assume the simultaneous formation of hydrocarbonate and hydroxide ions. Indeed, during cooling of the composite, the initial mixture can recrystallize into several phases combining alkaline metal cations from the eutectic and formed hydroxide ions. Thus as hydroxides are mixed with ternary LiNaK eutectic, it is well-known that the recrystallization temperature can be decreased, which could correspond to the second drop in conductivity around 360 °C [58,59], as shown in Figure 3b.

The next drop could be ascribed to NaOH formation as its recrystallization temperature is lower, around 310 °C [60].

Furthermore, by increasing the amount of hydrogen in the atmosphere, even if no change is observed during the first heating, it is worth noting that both transition temperatures during the first cooling are slightly shifted towards a lower temperature, as illustrated in Figure 4a,b. This is confirmed during the second heating/cooling cycle as reported in Figure 4c,d. This corroborated the change of molten phase composition, from molten carbonate to molten carbonate-hydroxide mixture, amplified by the increase in the amount of hydrogen in the surrounding atmosphere; thus displacing the equilibrium (Reactions (3) and (4)) to the right side and, consequently, favoring the transformation of carbonate into hydroxides ions. Slight decreases in activation energies can be noticed as a result of easier transports, thanks to higher amounts of hydrogen in the atmosphere, according to Reaction (2).

The previous description finally involves extrinsic defects, thus not initially included in the material. This notion of extrinsic ionic conduction was first suggested by Marques et al. [48], whereas Zhu et al. [61,62] developed a conduction by protons, as well as Huang et al. [23]. The role of the carbonate ion has been elucidated next by Wang et al. [34] and more deeply in numerous studies [63–65]. Following this approach, proton interacts with both oxide and carbonate ions through metastable hydrogen bonds, thus the rotation and the mobility of carbonate ion favors proton mobility, breaking these metastable bonds. Above the melting temperature, this mobility is important enough to ensure high conductivity of composite material, with a low activation energy. Moreover, the recent works of Xiong et al. [57] showed experimentally for BZY-$(Li,Na)_2CO_3$, in parallel with DFT calculations, that hydrocarbonates were the preferential species involving protons in carbonates, more specifically at the interface with the oxide phase, according to Reaction (4).

Dealing with the transition temperatures (t_t), their corresponding values were also determined by DSC analyses, in order to corroborate the assumptions based on the impedance spectroscopy results. In Figure 5, DSC signals are reported during two thermal cycles, in pure argon and in hydrogen-containing dry atmospheres (23 %vol. and 50 %vol. in Ar), for the same sample. It could be noted, compared to pure Ar, a progressive decrease in the recrystallization temperature of the ternary eutectic was observed by increasing the hydrogen content, with Δt = 20 and 27 °C, for 23% and 50% of H_2 in Ar, respectively, whereas the melting temperature is not affected by the atmosphere composition. Furthermore, some additional peaks appear during the first cooling around 368–365 °C, independent of the hydrogen content. It could be linked to KOH recrystallization, with a melting temperature being 400 °C [60]. Another peak after the main one, according to the screening direction, appears at 309–307 °C. It is also non-dependent of the hydrogen content and could be ascribed to NaOH recrystallization, as the melting temperature is close to 320 °C [60]. It is worth noting that the presence of hydroxide is well-known to induce a lowering of melting temperature of the LiNaK carbonate mixture [58,59], as observed in the Figure 5b,d during both cooling steps for the recrystallization temperature, as well as in Figure 5c, during the second heating after modification of the molten salts composition.

During the second heating, three peaks can be distinguished. The first one, exothermic, is not explained. The second one, endothermic, corresponds to the melting of one phase, more probably ascribed to sodium hydroxides as already assumed (transition temperature around 313–315 °C), not dependent on the hydrogen content even during melting. However, the peak which could have been related to the melting of potassium carbonate as this recrystallized phase has been identified during the first cooling, is not evidenced due to the probable overlapping of this peak with the enlarged eutectic melting DSC signal. Moreover, during the second heating, the higher the hydrogen content, the lower the eutectic melting temperature: 362 and 354 °C for 23% and 50% of H_2 in Ar, respectively, compared to initial 389 °C (first heating step). As during these DSC signal acquisitions, the temperature rate is quite low (2 °C·min^{-1}), the hydrogen oxidation obviously can occur and forms some hydroxide and hydrocarbonate ions as previously described (Reaction (4)). Table 2

summarizes all the phase transition temperatures revealed by DSC measurements as a function of the atmosphere composition and the step in the cycling.

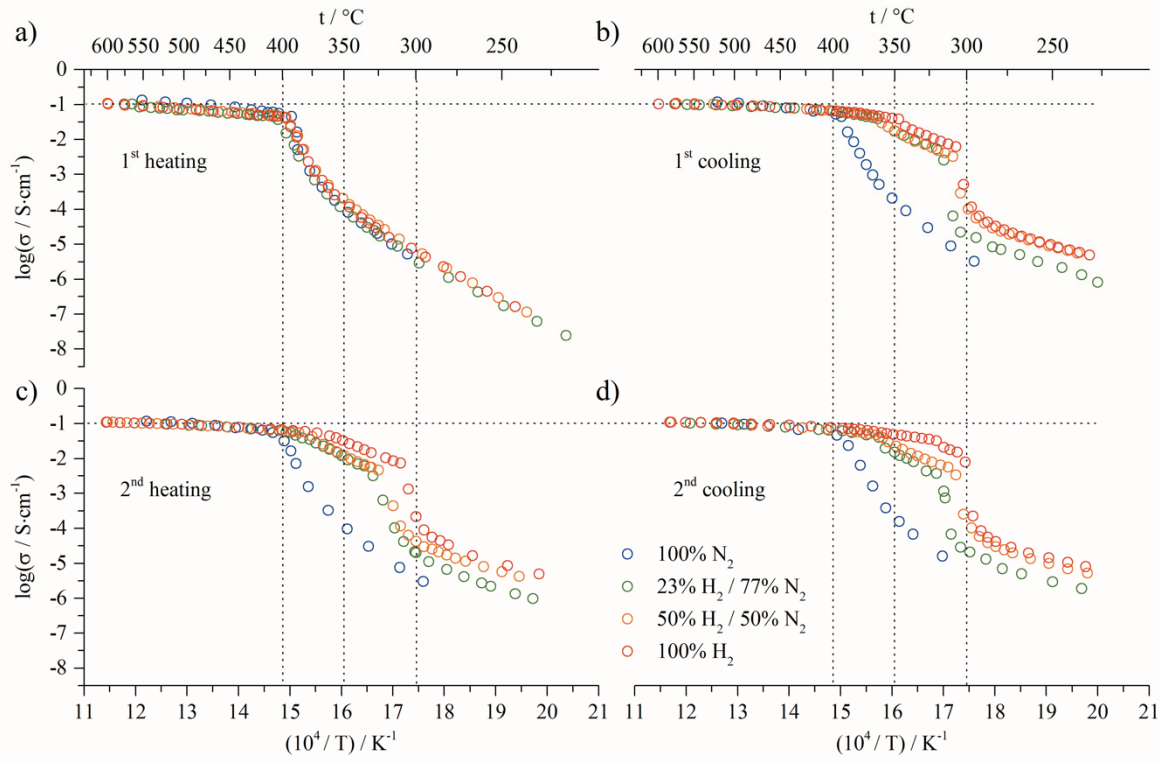

Figure 4. Impact of H_2 content diluted in dry N_2 (from 0 to 100 %vol.) on the electrical stability of the SDC—LiNaK composite. Arrhenius diagrams correspond to each part of a cycle and are shown separately: (**a**) 1st heating; (**b**) 1st cooling; (**c**) 2nd heating; and (**d**) 2nd cooling.

Table 2. Transition temperature (t_{onset}) dependence on H_2 percentage in Ar for SDC—LiNaK electrolyte powder detected by DSC studies during one or two heating/cooling scanning cycles. All peaks are endothermic during heating if the opposite is not indicated; all peaks are exothermic during each cooling stage.

SDC-LiNaK	Gas Mixture	t_{onset}, °C		
		H_2, %vol. in Ar		
		0	23	50
1st cycle	Heating	387	389	389
	Cooling	385	379	380
		377	365	358
		-	307	309
2nd cycle	Heating	-	302 (exo)	297 (exo)
			313	315
			362	354
	Cooling	-	379	378
			363	347
			309	311

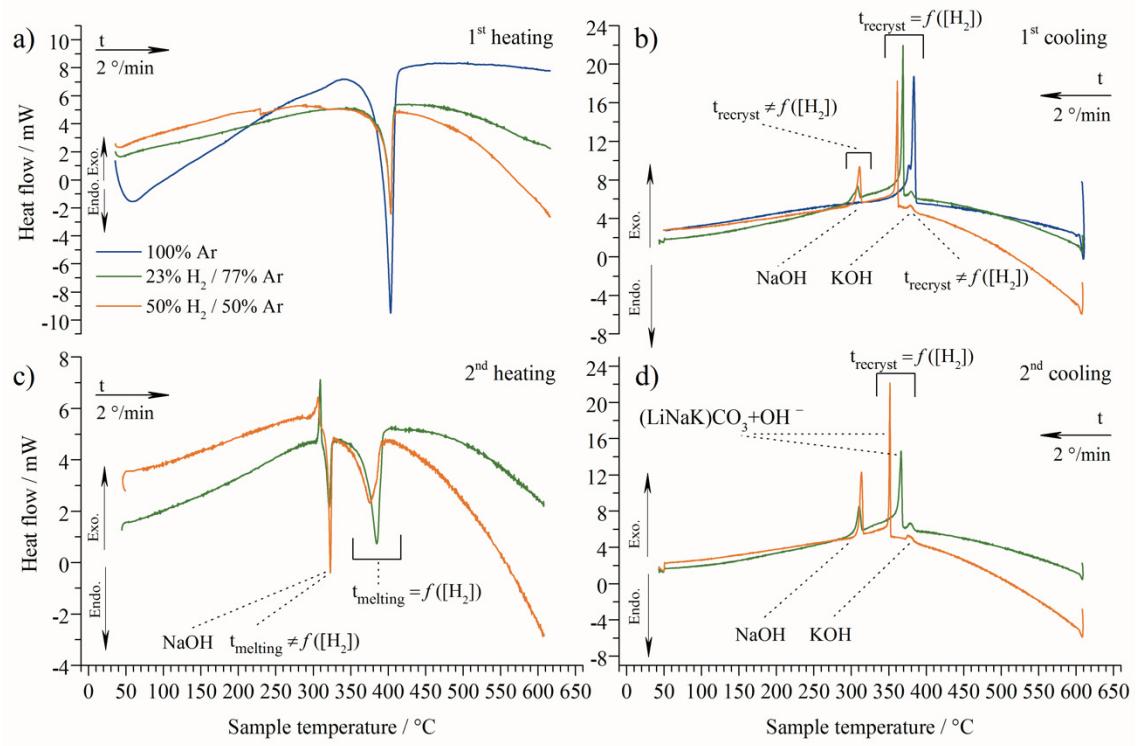

Figure 5. DSC signals observed for SDC—LiNaK electrolyte powder as function of sample temperature in pure Ar, 23%— and 50%—H_2—in—Ar gas mixtures at atmospheric pressure. The first heating/cooling cycle (**a**,**b**) was followed by second one (**c**,**d**) for the same sample. Scanning rate was two degrees per minute and its direction is indicated by arrows.

Thanks to the previous observations, if carbonates are partially transformed into hydroxides, in hydrogen-based surrounding atmospheres, the corresponding reactions can be written as Reactions (5) and (6). This will first be induced by the partial reduction in hydrogen of Ce^{4+} into Ce^{3+}, thus to electron creation and, as a direct reaction, the formation of water molecules. As a result of the presence of H_2O, some carbonate ions will react and lead to the formation of CO_2, and hydroxide ions. As CO_2 is produced this could explain that decarbonation, i.e., the transformation of carbonates into oxide ions is avoided (Reactions (6)–(8)), displacing equilibrium and stabilizing the system. It is worth noting that this phenomenon was one of the controversies when discussing the apparent stability of these materials, operating without adding CO_2 in the surrounding atmospheres. In the usual MCFC, there is no possible reduction, probably as the lithium aluminate porous matrix is inert whatever the operating atmosphere, thus no electrons are produced and next to no CO_2 is formed. Therefore CO_2 is required in both atmospheres in the hybrid system. Moreover, in the current composite materials, it is worth mentioning that these electrons are not mainly introducing electronic conductivity into the composite electrolyte; they induce partial transformation of molten carbonates into hydroxide ions, leading to lower transition temperature during the first cooling step, stabilizing it as no change in the electrical behavior is observed.

$$2CeO_2 + H_2 \leftrightarrow Ce_2O_3 + H_2O \quad (5)$$

$$H_2O + CO_3^{2-} \leftrightarrow CO_2 + 2OH^- \quad (6)$$

$$H_2 + 2CO_3^{2-} \leftrightarrow 2CO_2 + 2OH^- + 2\bar{e} \quad (7)$$

$$CO_3^{2-} \leftrightarrow CO_2 + O^{2-} \quad (8)$$

More interesting is the impact of water addition in oxygen-based and hydrogen-based atmospheres, as reported in Figure 6a,b, respectively. The electrical behavior in such moist atmospheres confirms the assumption of hydroxide formation, as added water favors the transformation of carbonates into hydroxides (Reaction (6)), even when no H_2 is initially present in the water-containing atmosphere (humid air). A hysteresis can be described in humid air, (Figure 6a) between the first heating and the other cycle steps even if its amplitude is not as important as in dry or humid hydrogen. The hysteresis is amplified when comparing the electrical behavior in dry hydrogen and humid hydrogen. The transition temperatures are shifted towards a lower temperature, whatever the moist atmosphere compositions. However, as previously concluded when dry atmospheres were surrounding the system, the composite material is transformed by the addition of water vapor in the atmospheres, yet almost stabilized after the first thermal cycle.

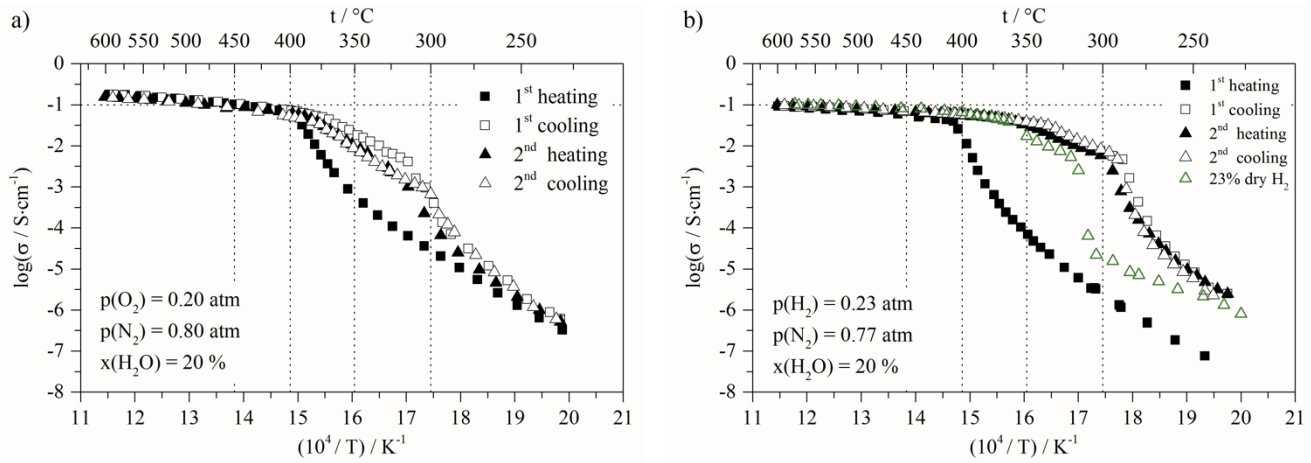

Figure 6. Influence of H_2O addition on electric behavior and stability of SDC—LiNaK composite electrolyte in: (**a**) oxidizing atmosphere (moistened synthetic air) and (**b**) reducing atmosphere (moistened 23%—H_2—in—N_2 mix). Arrhenius diagrams represent two heating/cooling cycles for both atmospheres. Symbols indicating the dry hydrogenated atmosphere (dry 23%—H_2—in—N_2) correspond to first cooling step on Figure 4b.

Coming back to the role of the interface, the phenomenon can be described once again by defect chemistry according to the Kröger–Vink notation by Reactions (9) and (10), for humidified air and completed with Reaction (11) in humidified hydrogen. In the later reaction, one can notice that hydrogen is also a resulting product allowing the mechanism repetition [66].

$$H_2O_{(g)} + V_O^{\bullet\bullet} + O_O^{\times} \leftrightarrow 2(OH)_O^{\bullet} \quad (9)$$

$$H_2O_{(g)} + V_O^{\bullet\bullet} + (CO_3)_{CO_3}^{\times} \leftrightarrow (OH)_O^{\bullet} + (HCO_3)_{CO_3}^{\bullet} \quad (10)$$

$$H_2O_{(g)} + V_O^{\bullet\bullet} + 2Ce_{Ce}' \leftrightarrow 2Ce_{Ce}^{\times} + O_O^{\times} + H_{2(g)} \quad (11)$$

Whatever the surrounding humidified atmosphere, hydroxyl and hydrocarbonate ions are formed, thus leading to specific conduction and the activation energies in the intermediate temperature range are still around 0.5 eV and 1.1 eV as described for the electrical behavior in dry hydrogen (Figure 3b). It is less evidenced in humidified air due to a shorter temperature range, although still present (Figure 6a).

Considering the addition of CO_2 in both reducing and oxidizing atmospheres, as in MCFC working atmosphere conditions, no more hysteresis is observed during heating and cooling cycles (Figure 7). This means that CO_2 is the required component in the atmosphere to fully stabilize the electrical behavior of molten carbonate/cerium-based solid oxide phase composite materials; as potential electrolytes, as shown by Reaction (8), avoiding eutectic decarbonation. Nevertheless, it should be noted that above the carbonate ternary eutectic melting temperature, the electrical conductivity is slightly higher in an oxidizing

atmosphere compared to the associated value in a reducing atmosphere, i.e., at 550 °C 0.17 S·cm^{-1} compared to 0.07 S·cm^{-1}, and at 600 °C 0.20 S·cm^{-1} compared to 0.10 S·cm^{-1}, respectively, combined also with some modifications of the activation energies. Referring to Rondão et al. [64] who studied the electrical behavior of CeO_2-$(Li,Na)_2CO_3$ composite in different atmospheres, they found that the conductivities vary in the following order $\sigma(H_2) > \sigma(O_2) > \sigma(CO_2)$. Taking into account that conductivity values in oxygen and carbon dioxide are much closer, they assumed that this conductivity decrease in CO_2 atmosphere could be the result of dicarbonate ion $C_2O_5^{2-}$ formation, according to Reaction (12):

$$CO_3^{2-} + CO_2 \leftrightarrow C_2O_5^{2-} \quad (12)$$

This possible transformation and the existence of dicarbonate ions as reported in [67–69], leads to a lower carbonate ions concentration, as well as a decrease in mobility of charge transport spaces due to the larger size of dicarbonate ions, resulting in an increase in activation energy and a decrease in conductivity in such operating conditions including CO_2.

Moreover, dealing with the stability of SDC-LiNaK in these surrounding atmospheres, in particular in a mixture of water, hydrogen and carbon dioxide (MCFC standard anode atmosphere), one can assume that it is due to the chemical stability of carbonate phase in the composite. Even if cerium can be reduced by H_2, different reactions can occur as already discussed, mainly the hydrogen oxidation in the presence of carbonate ions, as well as carbonates hydrolysis in the presence of water according to Reactions (6) and (7), respectively. The chemical stability is maintained thanks to the high partial pressure of CO_2 on the MCFC anodic atmosphere: 16 %vol. of CO_2 seems to permit the displacement of both 6 and 7 reaction equilibria, avoiding the formation of hydroxides and thus the recrystallization into new phases during the cooling.

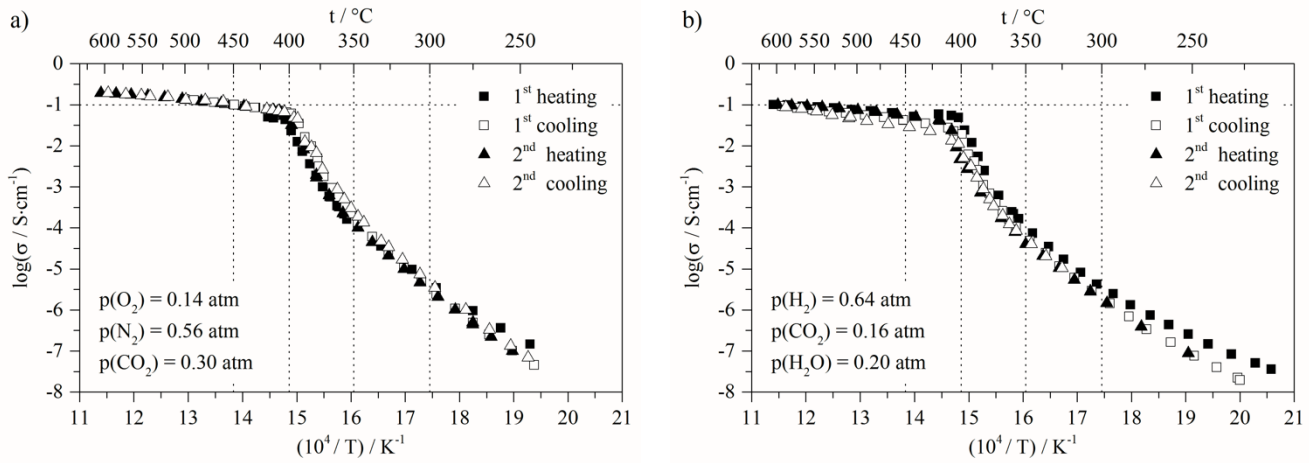

Figure 7. Influence of CO_2 addition on electric behavior and stability of SDC—LiNaK composite electrolyte in: (**a**) oxidant compartment and (**b**) reducing compartment of a Molten Carbonate Fuel Cell (MCFC) operated in standard conditions. Arrhenius diagrams represent two heating/cooling cycles for both MCFC simulated atmospheres.

X-ray diffraction analysis was performed on the as-synthesized pellet, and after impedance spectroscopy measurements in the different atmospheres as reported and discussed before. Sm-doped ceria is indexed as cubic structure (Fm3m) with the well-defined more intense and narrow peaks (Figure 8a,b). Nevertheless, the complete indexation is highly complex due to numerous small peaks corresponding to the carbonates and new phases appearing after exposition during several thermal cycles. This also explains the specific representation of the square root of the intensity recorded. Moreover, some assumed new phases based on carbonates, hydrogen carbonates, hydroxides and other potential and especially non-stoichiometric phases are not systematically referenced in XRD data bases, or with low accuracy.

Nevertheless, from obtained diffractograms we can clearly distinguish the change in phase composition of initial SDC-LiNaK after thermal cycling and recrystallization under reducing atmospheres (Figure 8a). Atmosphere containing 23 %vol. of hydrogen generally induces the recrystallization of the same phases forming the initial eutectic mixture. At the same time, some new diffraction maxima appear, although their indexation remains problematic due to low intensity. This new phase can be more precisely indexed in the case of 100 %vol. hydrogen atmosphere as $NaK_2[H(CO_3)_2]\cdot 2H_2O$ (PDF n° 04-010-8201). It is important to highlight that such a phase modification process goes with the SDC grain's coalescence, which is much stronger at higher H_2 content. The micrographs obtained by Scanning Electron Microscopy (Figure 9c,e,f) show this influence, which results in the growing up of the oxide phase into larger grains, thus reducing the interfacial oxide-carbonate surface, and making the phase distribution homogeneity much less favorable. This phenomenon is reflected by a decrease in the SDC phase full width at half-maximum (FWHM) on corresponding XRD patterns (Figure 8a). The same $NaK_2[H(CO_3)_2]\cdot 2H_2O$ phase is formed in larger amounts in the sample exposed to humidified 23 %vol.-H_2, which leads us to the same conclusion that the presence of water promotes the formation of hydrogenated carbonate phases in the composite electrolyte mixture. These results corroborate the conclusions drawn from Arrhenius diagrams obtained during thermal cycling under the same atmospheres. In addition, in the case of humidified air (Figure 8b) water itself can induce recrystallization of the same hydrogenated phase, as well as others, such as $Na_3[H(CO_3)_2]\cdot 2H_2O$ (PDF n° 00-029-1447) and $KHCO_3$ (PDF n° 04-013-5503) compared with dry air. Interesting to note that in the two cases of these humidified atmospheres (containing hydrogen or not), the microstructure does not undergo any significant changes (Figure 9b,d) except a slight increase in SDC phase grain size. However, this oxide phase remains well-dispersed throughout the volume of the composite material. This indirectly suggests an important role of ceria reduction process by H_2 and its re-oxidation in the presence of water according to Reaction (11).

With regard to the standard operating MCFC atmospheres, the cathode-one (30 %vol. CO_2 in air) is not a source of a significant change in recrystallized phases compared to the initial electrolyte composition. The same phases are found in the sample resulting from the synthesis, as well as in that which has undergone thermal cycling in dry air. However, certain maxima present on the XRD pattern could indicate the presence of a hydrogenated carbonate phase, in particular $NaK_2[H(CO_3)_2]\cdot 2H_2O$. However, it is difficult to pronounce this as there are not as many maxima that can be attributed to this suspected phase, and compared to the sample studied under humidified air (where this phase is undoubtedly present), some are even absent. So, it could be another composition that is not listed in the database.

Moreover, the standard MCFC anode atmosphere (64 %vol. H_2/16 %vol. CO_2/20 %vol. H_2O), induces a low recrystallization of $NaK_2[H(CO_3)_2]\cdot 2H_2O$, which is certainly due to the presence of hydrogen. Nevertheless, a diffraction maximum at 90.5°2θ remains unexplained. In addition, the formation of a sodium oxalate phase can be suspected after cycling under this atmosphere. Usually, oxalate ions can only be formed in the presence of carbon monoxide (Reaction (13)) in the surrounding atmosphere, which is not the case. Furthermore, the chromatographic analysis based on a protocol fixed by Meskine et al. [70] indicates the presence of CO in the outlet gas mix (cf. Supplementary Information). It can be assumed here that the formation of CO can be catalytically favored in the presence of samaria-doped ceria in the composite according to the reverse water gas shift reaction (RWGS) (Reaction (14)) [71].

$$CO_3^{2-} + CO \leftrightarrow C_2O_4^{2-} \quad (13)$$

$$CO_2 + H_2 \leftrightarrow CO + H_2O \quad (14)$$

The composite electrolyte morphology of sample cycled in standard MCFC cathodic atmosphere does not present any notable differences compared to the as-synthetized sample. It could be suggested that there are no chemical interactions between the phases making

up the composite material under such conditions. The absence of this type of reactivity is systematically mentioned in the literature [17,72]. Referring to the last micrograph obtained for a sample being cycled under anodic MCFC atmosphere (Figure 9h), we can conclude that such conditions prove to be very favorable regarding the stability of the initial microstructure of the SDC-LiNaK composite, or even its slight improvement in terms of homogeneity of the phase distribution compared to the as-synthesized sample. It is clear that this structural stability of the electrolyte is partly responsible for the stable behavior during thermal cycling under such an atmosphere, and this positively influences its electrical behavior. Here, one may assume that a sufficient partial pressure CO_2 level plays a protective role, thus preventing the equilibrium displacement in the decarbonation direction of the composite material (Reaction (8)).

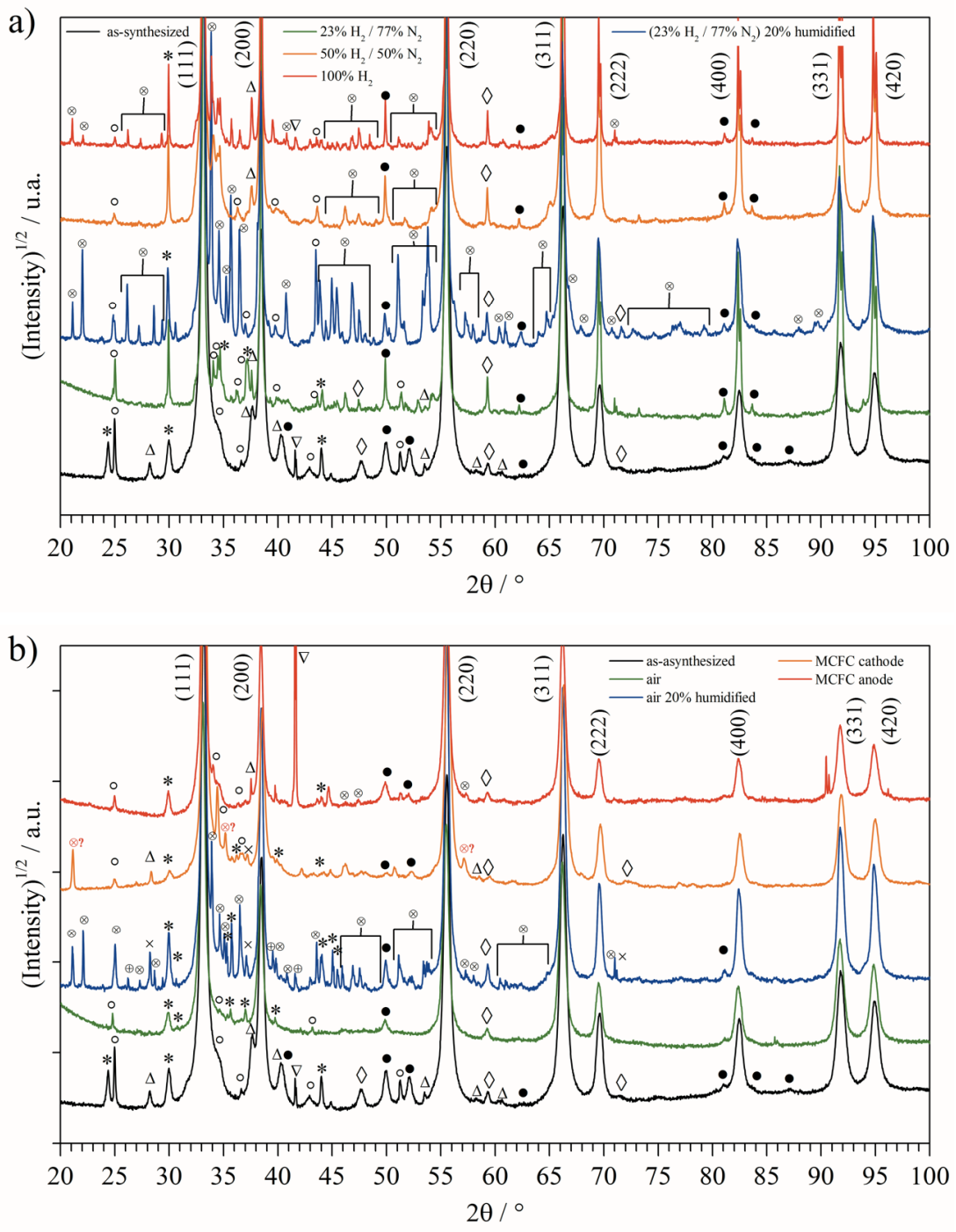

Figure 8. (**a**)—X-ray diffraction patterns of SDC—LiNaK electrolyte after operation in reducing

atmospheres: dry or wet, different content of H_2 diluted in N_2 (from 23 to 100 %vol). (**b**)—X-ray diffraction patterns after operation in oxidizing and standard MCFC atmospheres. Patterns of the as-synthesized pellet is reported as a reference on both (**a**) and (**b**) figures. °—Li_2CO_3 (PDF n° 04-008-0471); •—Na_2CO_3 (PDF n° 04-010-2762); ∗—K_2CO_3 (PDF n° 00-049-1093); Δ—$NaLiCO_3$ (PDF n° 00-021-0954); ◊—$KNaCO_3$ (PDF n° 00-001-1038); ⊗—$NaK_2[H(CO_3)_2]\cdot 2H_2O$ (PDF n° 04-010-8201); ∇—$Na_2C_2O_4$ (PDF n° 04-013-1742); ⊕—$Na_3[H(CO_3)_2]\cdot 2H_2O$ (PDF n° 00-029-1447); ×—$KHCO_3$ (PDF n° 04-013-5503). Indexed maxima correspond to samaria-doped ceria phase: $Ce_{0.8}Sm_{0.2}O_{1.9}$ (PDF n° 04-013-0036).

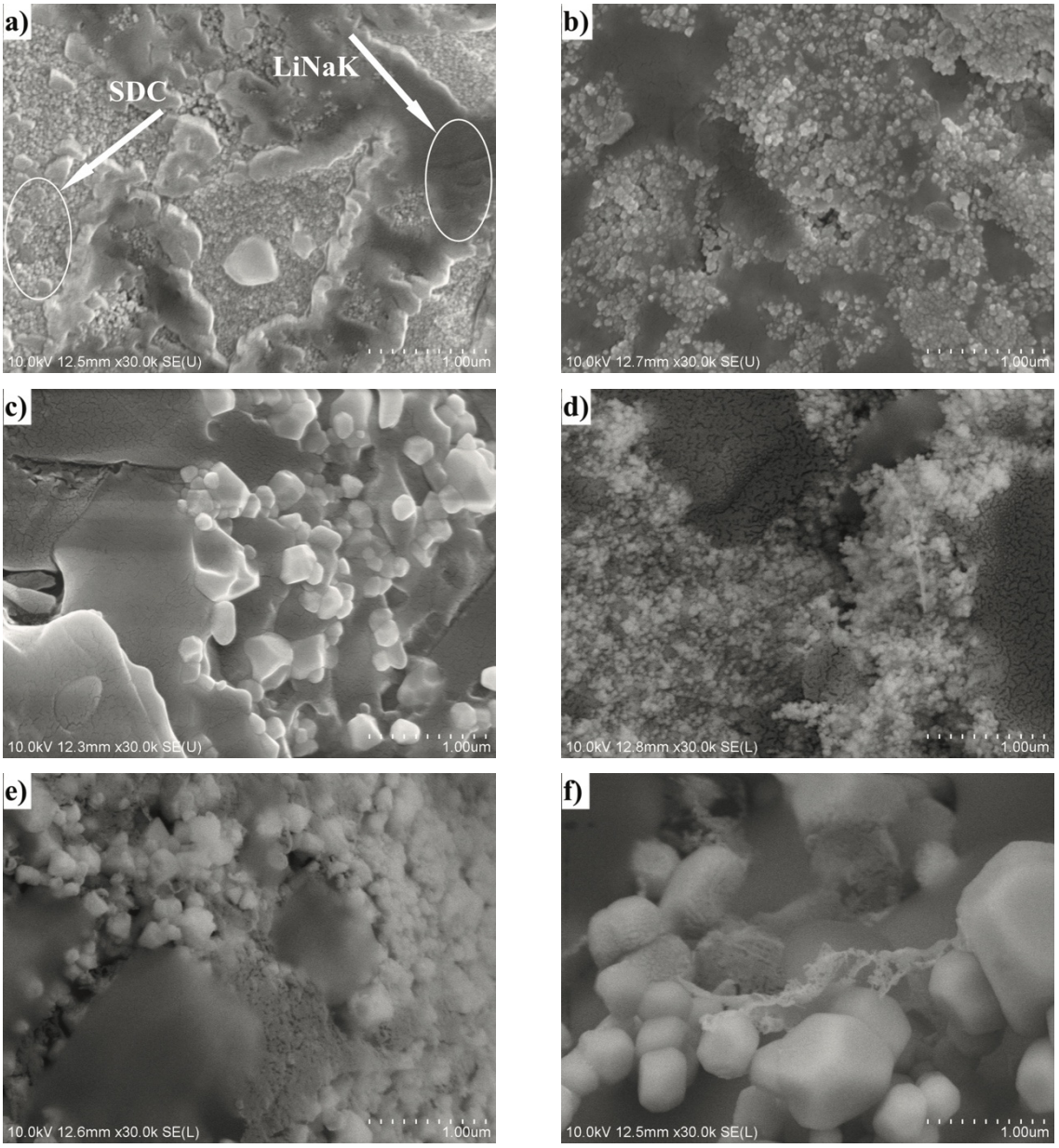

Figure 9. *Cont*.

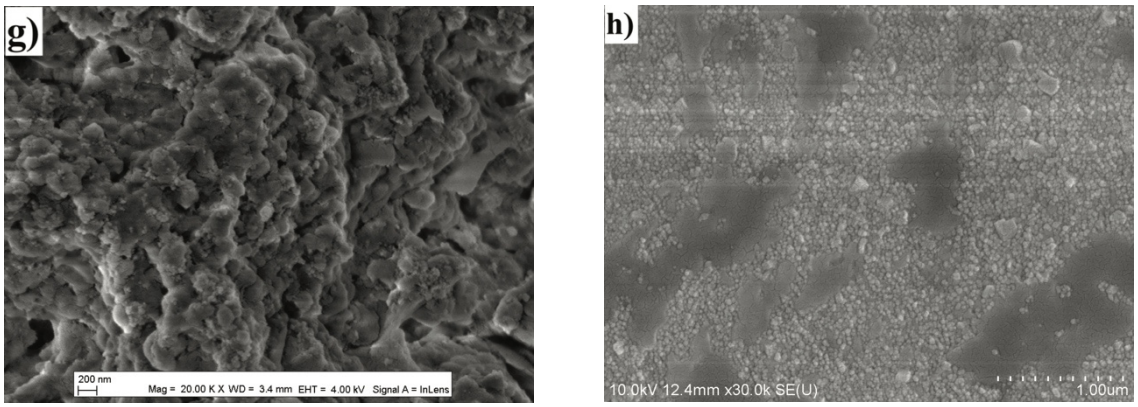

Figure 9. SEM micrographs obtained from samples of SDC—LiNaK composite electrolyte after synthesis (**a**) and after thermal cycling EIS experiments under 20%—humidified synthetic air (**b**); dry (**c**) and humid (**d**) 23%-H_2-in-N_2; dry 50%-H_2-in-N_2 (**e**); dry 100% H_2 (**f**); and under MCFC simulated cathodic (**g**) and anodic (**h**) atmospheres.

EIS experiments are corroborated by DSC measurements in the same atmospheres when possible. These results indicate the formation of alkali hydroxides (NaOH and KOH) in amounts small, yet sufficient when mixed to carbonate eutectic, to reduce their melting temperature, initiating then the appearance of transition temperatures in the low temperature region (250–350 °C). Thus, a combination of these two experimental methods allowed us to review and establish, in the form of chemical equations, different possible interactions between the phases, constituting the composite electrolyte and surrounding atmospheres, while considering the predominant role of the oxide/carbonate interface in the formation of various ionic species responsible for the total conductivity of the electrolyte material. These equations are summarized in Figure 10.

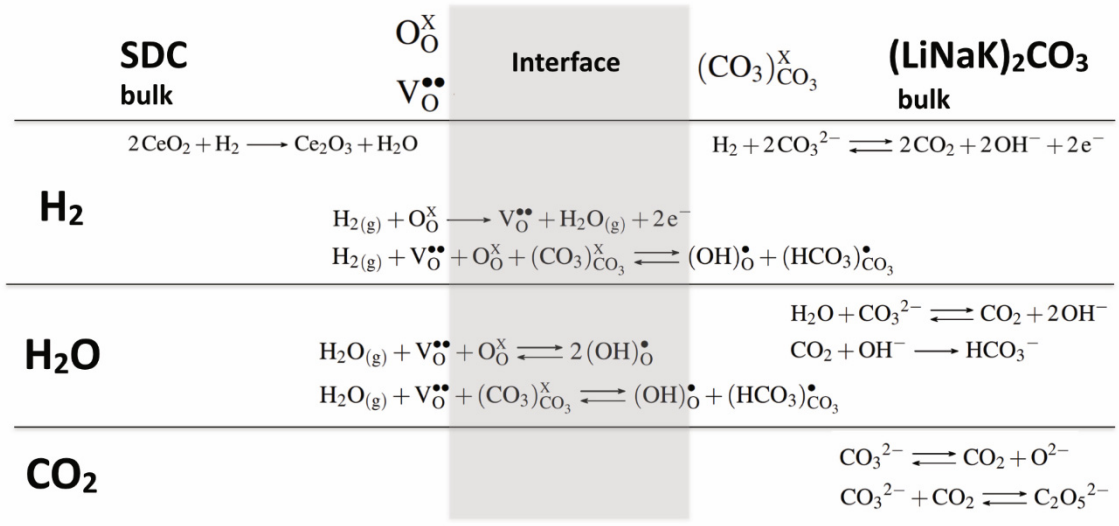

Figure 10. Summary of the mechanistic model for the transport mechanisms and phenomena at the solid oxide/molten carbonate interface.

It is important to highlight that MCFC standard operating atmospheres do not strongly affect the conductivity of composite SDC-LiNaK electrolyte whatever the temperature range, except a slight decrease in the conductivity values in 400–550 °C range during thermal cycling in standard anodic atmosphere. This fact is likely to be assigned to dicarbonate ion formation at high CO_2 partial pressures. Therefore, it probably can be recommended during fuel cell operation, employing any composite oxide/carbonate electrolyte, to keep the CO_2 partial pressure at an optimal level on both cathode and anode compartments.

4. Conclusions

This study achieved a deeper understanding of the electrical behavior and thermal stability issues of SDC-LiNaK composite electrolyte under various reducing, oxidizing, wet and dry atmospheres. Impedance Electrochemical Spectroscopy coupled to thermal cycling, directly provided information about electrolyte conductivity values, activation energy values and their changes (variations) throughout at least two complete heating/cooling cycles in an intermediate temperature range (250–600 °C). SDC-LiNaK composite underwent different hydrogen contents; dry reducing atmospheres highlight a different electrical behavior during a cooling stage at the end of the first thermal cycle. It consists of the occurrence of different transition temperatures separating Arrhenius plots in different regions characterized by singular activation energy values. The more the surrounding atmosphere is rich in hydrogen, the greater the shift in transition temperatures toward lower temperatures. This transformation becomes remarkable when the electrolyte is exposed to humidified 23%-in N_2-hydrogen mixture. Moreover, it was shown that water, present in air, forming a humidified oxidizing atmosphere, induces the same changes in SDC-LiNaK electrical behavior. Thus, in both dry and wet hydrogenated atmospheres, an Arrhenius plot high temperature region (350–600 °C) appears with an activation energy value around 0.45 eV, which indicates a conductivity mechanism involving hydrogenated ions.

Post mortem phase composition results reinforce our conclusions on conduction mechanisms revealed by EIS measurements. Indeed, during recrystallization at the final cooling stage, new hydrogen carbonate phases are formed in hydrogen- and/or water-content atmospheres: $KHCO_3$, $Na_3[H(CO_3)_2]\cdot 2H_2O$ and $NaK_2[H(CO_3)_2]\cdot 2H_2O$. Concerning samples undergoing MCFC standard operation atmospheres, the phase composition remains generally stable, except with regard to sodium oxalate formation in anodic atmosphere, due to a reverse water gas shift reaction (RWGS) manifestation and the resulting CO formation and its subsequent interaction with carbonate ions.

Morphological studies indicate a tangible change in the microstructure of electrolyte samples thermally cycled in hydrogen-content dry atmospheres: the oxide phase grains coalesce, and the process is more amplified with higher hydrogen content. Water prevents transformations of this oxide phase whatever the atmosphere used. In contrast, carbon dioxide-content and both MCFC standard operating atmospheres do not affect the SDC-LiNaK composite microstructure.

Finally, the authors expect that the present results on the electrical behavior and thermal stability of SDC-LiNaK can be extrapolated over a large family of composite oxide/carbonate electrolytes.

Supplementary Materials: The following supporting information can be downloaded at: https://www.mdpi.com/article/10.3390/en15072688/s1, Figure S1: Outlet composition of gas mixture during EIS thermal cycling analysis of SDC-LiNaK under MCFC standard reducing conditions at 441 °C and 546 °C. Table S1: Retention times of gases forming an outlet mixture during EIS thermal cycling analysis of SDC-LiNaK under MCFC standard reducing conditions. Figure S2. Nyquist EIS plots recorded in nitrogen atmosphere at different temperatures within the symmetric Au | SDC-LiNaK | Au electrochemical configuration. The amplitude of the applied sinusoidal voltage was V_0 = 100 mV. The numbers on the diagrams indicate the logarithm of the frequency of the applied signal. Table S2. Activation energy (E_a) and transition temperature (t_t) values calculated from Arrhenius plot during thermal cycling of SDC-LiNaK under dry reducing atmospheres containing different amounts of hydrogen. H—heating; C—cooling; LT and HT—low and high temperature regions respectively. Table S3. Activation energy (E_a) and transition temperature (t_t) values calculated from Arrhenius plot during thermal cycling of SDC-LiNaK under oxidizing and reducing atmospheres both containing 20% of moisture. H—heating; C—cooling; LT and HT—low and high temperature regions respectively. Table S4. Activation energy (E_a) and transition temperature (t_t) values calculated from Arrhenius plot during thermal cycling of SDC-LiNaK under MCFC standard oxidizing and reducing atmospheres. H—heating; C—cooling; LT and HT—low and high temperature regions respectively.

Author Contributions: Conceptualization, A.G. and A.R.; Data curation, A.G.; Funding acquisition, A.R.; Investigation, A.G. and M.B.O.; Methodology, A.G., M.B.O., H.M. and V.A.; Project administration, A.R.; Supervision, A.R.; Validation, V.L., M.C. and A.R.; Writing—review and editing, A.G., M.B.O., V.L. and A.R. All authors have read and agreed to the published version of the manuscript.

Funding: This research was funded by PSL (Paris Sciences et Lettres) for A. Grishin and H. Meskine Ph.D. grants and ANR EQUIPEX (PLANEX ANR-11-EQPX-0-01) for DSC/TGA facilities.

Institutional Review Board Statement: Not applicable.

Informed Consent Statement: Not applicable.

Conflicts of Interest: The authors declare no conflict of interest.

References

1. Zhu, B.; Mellander, B.E. Proton Conduction in Nitrate-Based Oxides and Related Ceramics at Intermediate Temperatures. *Solid State Ion.* **1994**, *70*, 285–290. [CrossRef]
2. Ricca, C.; Albin, V.; Labat, F.; Adamo, C.; Cassir, M.; Ringuedé, A. A First Combined Electrochemical and Modelling Strategy on Composite Carbonate/Oxide Electrolytes for Hybrid Fuel Cells. *Int. J. Hydrog. Energy* **2016**, *41*, 18778–18787. [CrossRef]
3. Jaiswal, N.; Upadhyay, S.; Kumar, D.; Parkash, O. Ca^{2+} and Sr^{2+} Co-Doped Ceria/Carbonates Nanocomposites for Low Temperature Solid Oxide Fuel Cells: Composite Effect. *Ceram. Int.* **2015**, *41*, 15162–15169. [CrossRef]
4. Jaiswal, N.; Upadhyay, S.; Kumar, D.; Parkash, O. Enhanced Ionic Conductivity in La^{3+} and Sr^{2+} Co-Doped Ceria: Carbonate Nanocomposite. *Ionics* **2015**, *21*, 2277–2283. [CrossRef]
5. Ahmed, A.; Raza, R.; Khalid, M.S.; Saleem, M.; Alvi, F.; Javed, M.S.; Sherazi, T.A.; Akhtar, M.N.; Akram, N.; Ahmad, M.A.; et al. Highly Efficient Composite Electrolyte for Natural Gas Fed Fuel Cell. *Int. J. Hydrog. Energy* **2016**, *41*, 6972–6979. [CrossRef]
6. Asghar, M.I.; Jouttijärvi, S.; Lund, P.D. High Performance Ceramic Nanocomposite Fuel Cells Utilizing LiNiCuZn-Oxide Anode Based on Slurry Method. *Int. J. Hydrog. Energy* **2018**, *43*, 12797–12802. [CrossRef]
7. Tanwar, K.; Jaiswal, N.; Sharma, P.; Kumar, D.; Parkash, O. Structural Analysis of Ce0.83Dy0.14Ca0.03O1.90(CDC) and Enhanced Electrical Conductivity of Its Composites with Alkali Carbonates for LT-SOFCs. *J. Alloy. Compd.* **2018**, *741*, 532–541. [CrossRef]
8. Singh, M.; Singh, A.K. Space Charge Layer Induced Superionic Conduction and Charge Transport Behaviour of "Alkali Carbonates and Tri-Doped Ceria Nanocomposites" for LT-SOFCs Applications. *Ceram. Int.* **2021**, *47*, 1218–1228. [CrossRef]
9. Zhu, B. Advantages of Intermediate Temperature Solid Oxide Fuel Cells for Tractionary Applications. *J. Power Sources* **2001**, *93*, 82–86. [CrossRef]
10. Zhu, B.; Mellander, B.E. Performance of intermediate temperature SOFCs with composite electrolytes. In *Solid Oxide Fuel Cells-VI*; Singhal, S.C., Dokiya, M., Eds.; The Electrochemical Society, Inc.: Pennington, NJ, USA, 1999; Volume 1999.
11. Fu, Q.X.; Zha, S.W.; Zhang, W.; Peng, D.K.; Meng, G.Y.; Zhu, B. Intermediate Temperature Fuel Cells Based on Doped Ceria-LiCl-$SrCl_2$ composite Electrolyte. *J. Power Sources* **2002**, *104*, 73–78. [CrossRef]
12. Slim, C.; Baklouti, L.; Cassir, M.; Ringuedé, A. Structural and Electrochemical Performance of Gadolinia-Doped Ceria Mixed with Alkali Chlorides (LiCl-KCl) for Intermediate Temperature-Hybrid Fuel Cell Applications. *Electrochim. Acta* **2014**, *123*, 127–134. [CrossRef]
13. Shi, R.; Chen, W.; Hu, W.; Liu, J.; Wang, H. $SrCe_{0.9}Sm_{0.1}O_3$-α compounded with NaCl-KCl as a Composite Electrolyte for Intermediate Temperature Fuel Cell. *Materials* **2018**, *11*, 1583. [CrossRef] [PubMed]
14. Sun, L.; Du, R.; Wang, H.; Li, H. Intermediate Temperature Electrochemical Properties of Yb^{3+} doped $SrCeO_{3\_}$ Carbonate and Chloride Composite Electrolytes. *Int. J. Electrochem. Sci.* **2018**, *13*, 5054–5060. [CrossRef]
15. Zhu, B. Functional Ceria–Salt-Composite Materials for Advanced ITSOFC Applications. *J. Power Sources* **2003**, *114*, 1–9. [CrossRef]
16. Zhu, B.; Mat, M.D. Studies on Dual Phase Ceria-Based Composites in Electrochemistry. *Int. J. Electrochem. Sci.* **2006**, *1*, 383–402.
17. Zhu, B.; Li, S.; Mellander, B.E. Theoretical Approach on Ceria-Based Two-Phase Electrolytes for Low Temperature (300–600 °C) Solid Oxide Fuel Cells. *Electrochem. Commun.* **2008**, *10*, 302–305. [CrossRef]
18. Yao, C.; Meng, J.; Liu, X.; Zhang, X.; Liu, X.; Meng, F.; Wu, X.; Meng, J. Enhanced Ionic Conductivity in Gd-Doped Ceria and $(Li/Na)_2SO_4$ Composite Electrolytes for Solid Oxide Fuel Cells. *Solid State Sci.* **2015**, *49*, 90–96. [CrossRef]
19. Wang, H.; Hu, T.; Xi, G. A Novel Gd^{3+} and Yb^{3+} Co-Doped Ceria-Sulphate Composite Electrolyte for Intermediate-Temperature Fuel Cells. *Ceram. Int.* **2020**, *46*, 8695–8699. [CrossRef]
20. Huang, J.; Gao, Z.; Mao, Z. Effects of Salt Composition on the Electrical Properties of Samaria-Doped Ceria/Carbonate Composite Electrolytes for Low-Temperature SOFCs. *Int. J. Hydrog. Energy* **2010**, *35*, 4270–4275. [CrossRef]
21. Jing, Y.; Lund, P.; Asghar, M.I.; Li, F.; Zhu, B.; Wang, B.; Zhou, X.; Chen, C.; Fan, L. Non-Doped CeO_2-Carbonate Nanocomposite Electrolyte for Low Temperature Solid Oxide Fuel Cells. *Ceram. Int.* **2020**, *46*, 29290–29296. [CrossRef]
22. Huang, J.; Yang, L.; Gao, R.; Mao, Z.; Wang, C. A High-Performance Ceramic Fuel Cell with Samarium Doped Ceria-Carbonate Composite Electrolyte at Low Temperatures. *Electrochem. Commun.* **2006**, *8*, 785–789. [CrossRef]
23. Huang, J.; Mao, Z.; Liu, Z.; Wang, C. Development of Novel Low-Temperature SOFCs with Co-Ionic Conducting SDC-Carbonate Composite Electrolytes. *Electrochem. Commun.* **2007**, *9*, 2601–2605. [CrossRef]

24. Huang, J.; Mao, Z.; Liu, Z.; Wang, C. Performance of Fuel Cells with Proton-Conducting Ceria-Based Composite Electrolyte and Nickel-Based Electrodes. *J. Power Sources* **2008**, *175*, 238–243. [CrossRef]
25. Huang, J.; Gao, R.; Mao, Z.; Feng, J. Investigation of La2NiO4+δ-Based Cathodes for SDC-Carbonate Composite Electrolyte Intermediate Temperature Fuel Cells. *Int. J. Hydrog. Energy* **2010**, *35*, 2657–2662. [CrossRef]
26. Gao, Z.; Mao, Z.; Wang, C.; Huang, J.; Liu, Z. Composite Electrolyte Based on Nanostructured $Ce_{0.8}Sm_{0.2}O_{1.9}$ (SDC) for Low-Temperature Solid Oxide Fuel Cells Zhan. *Int. J. Energy Res.* **2009**, *33*, 1138–1144. [CrossRef]
27. Yao, X.; Li, P.; Yu, B.; Yang, F.; Li, J.; Zhao, Y.; Li, Y. Hydrothermally Synthesized NiO-Samarium Doped Ceria Nano-Composite as an Anode Material for Intermediate-Temperature Solid Oxide Fuel Cells. *Int. J. Hydrog. Energy* **2017**, *42*, 22192–22200. [CrossRef]
28. Xia, C.; Li, Y.; Tian, Y.; Liu, Q.; Wang, Z.; Jia, L.; Zhao, Y.; Li, Y. Intermediate Temperature Fuel Cell with a Doped Ceria-Carbonate Composite Electrolyte. *J. Power Sources* **2010**, *195*, 3149–3154. [CrossRef]
29. Asghar, M.I.; Jouttijärvi, S.; Jokiranta, R.; Lund, P.D. Remarkable Ionic Conductivity and Catalytic Activity in Ceramic Nanocomposite Fuel Cells. *Int. J. Hydrog. Energy* **2018**, *43*, 1–8. [CrossRef]
30. Song, S.A.; Jang, S.C.; Han, J.; Yoon, S.P.; Nam, S.W.; Oh, I.H.; Lim, T.H. Enhancement of Cell Performance Using a Gadolinium Strontium Cobaltite Coated Cathode in Molten Carbonate Fuel Cells. *J. Power Sources* **2011**, *196*, 9900–9905. [CrossRef]
31. Li, S.; Sun, J. Electrochemical Performances of NANOCOFC in MCFC Environments. *Int. J. Hydrog. Energy* **2010**, *35*, 2980–2985. [CrossRef]
32. Benamira, M.; Ringuedé, A.; Hildebrandt, L.; Lagergren, C.; Vannier, R.N.; Cassir, M. Gadolinia-Doped Ceria Mixed with Alkali Carbonates for SOFC Applications: II—An Electrochemical Insight. *Int. J. Hydrog. Energy* **2012**, *37*, 19371–19379. [CrossRef]
33. Shilong, Y.; Zhupeng, Y.; Chuanming, L.; Xiaowei, C.; Yanwei, Z. Theoretical Description on the Interface-Enhanced Conductivity of SDC/LiNa-Carbonate Composite Electrolytes. *Mater. Lett.* **2013**, *92*, 78–81. [CrossRef]
34. Wang, X.; Ma, Y.; Li, S.; Kashyout, A.H.; Zhu, B.; Muhammed, M. Ceria-Based Nanocomposite with Simultaneous Proton and Oxygen Ion Conductivity for Low-Temperature Solid Oxide Fuel Cells. *J. Power Sources* **2011**, *196*, 2754–2758. [CrossRef]
35. Maier, J. Ionic Conduction in Space Charge Regions. *Prog. Solid State Chem.* **1995**, *23*, 171–263. [CrossRef]
36. Ricca, C.; Ringuedé, A.; Cassir, M.; Adamo, C.; Labat, F. Revealing the Properties of the Cubic ZrO_2 (111) Surface by Periodic DFT Calculations: Reducibility and Stabilization through Doping with Aliovalent Y_2O_3. *RSC Adv.* **2015**, *5*, 13941–13951. [CrossRef]
37. Ricca, C.; Medina-Lott, B.; Albin, V.; Labat, F.; Adamo, C.; Hinojosa, M.; Cassir, M.; Ringuedé, A. Hybrid Fuel Cells with Carbonate/Oxide Composite Electrolytes: An Electrochemical and Theoretical Insight. *ECS Trans.* **2015**, *68*, 2597–2609. [CrossRef]
38. Ricca, C.; Grishin, A.; Ringuedé, A.; Cassir, M.; Adamo, C.; Labat, F.; Saboungi, M.L.; Ringuedé, A. Modeling Composite Electrolytes for Low-Temperature Solid Oxide Fuel Cell Application: Structural, Vibrational and Electronic Features of Carbonate–Oxide Interfaces. *J. Mater. Chem. A* **2016**, *4*, 17473–17482. [CrossRef]
39. Ricca, C.; Ringuedé, A.; Cassir, M.; Ottochian, A.; Adamo, C.; Labat, F. Defect Formation and Diffusion on the (001) Surface of LiKCO3 for Fuel Cell Applications: Insight from Hybrid DFT. *J. Phys. Chem. C* **2016**, *120*, 12941–12951. [CrossRef]
40. Ricca, C.; Ringuedé, A.; Cassir, M.; Adamo, C.; Labat, F. Conduction Mechanisms in Oxide-Carbonate Electrolytes for SOFC: Highlighting the Role of the Interface from First-Principles Modeling. *J. Phys. Chem. C* **2018**, *122*, 10067–10077. [CrossRef]
41. Asghar, M.I.; Heikkilä, M.; Lund, P.D. Advanced Low-Temperature Ceramic Nanocomposite Fuel Cells Using Ultra High Ionic Conductivity Electrolytes Synthesized through Freeze-Dried Method and Solid-Route. *Mater. Today Energy* **2017**, *5*, 338–346. [CrossRef]
42. Zhao, Y.; Xia, C.; Wang, Y.; Xu, Z.; Li, Y. Quantifying Multi-Ionic Conduction through Doped Ceria-Carbonate Composite Electrolyte by a Current-Interruption Technique and Product Analysis. *Int. J. Hydrog. Energy* **2012**, *37*, 8556–8561. [CrossRef]
43. Xia, C.; Li, Y.; Tian, Y.; Liu, Q.; Zhao, Y.; Jia, L.; Li, Y. A High Performance Composite Ionic Conducting Electrolyte for Intermediate Temperature Fuel Cell and Evidence for Ternary Ionic Conduction. *J. Power Sources* **2009**, *188*, 156–162. [CrossRef]
44. Benamira, M.; Ringuedé, A.; Albin, V.; Vannier, R.N.; Hildebrandt, L.; Lagergren, C.; Cassir, M. Gadolinia-Doped Ceria Mixed with Alkali Carbonates for Solid Oxide Fuel Cell Applications: I. A Thermal, Structural and Morphological Insight. *J. Power Sources* **2011**, *196*, 5546–5554. [CrossRef]
45. Schober, T. Composites of Ceramic High-Temperature Proton Conductors with Inorganic Compounds. *Electrochem. Solid-State Lett.* **2005**, *8*, A199. [CrossRef]
46. Zhu, B. Next Generation Fuel Cell R&D. *Int. J. Energy Res.* **2006**, *30*, 895–903. [CrossRef]
47. Ferreira, A.S.V.; Saradha, T.; Figueiredo, F.L.; Marques, F.M.B. Compositional and Microstructural Effects in Composite Electrolytes for Fuel Cells. *Int. J. Energy Res.* **2011**, *35*, 1090–1099. [CrossRef]
48. Ferreira, A.S.V.; Soares, C.M.C.; Figueiredo, F.M.H.L.R.; Marques, F.M.B. Intrinsic and Extrinsic Compositional Effects in Ceria/Carbonate Composite Electrolytes for Fuel Cells. *Int. J. Hydrog. Energy* **2011**, *36*, 3704–3711. [CrossRef]
49. Lair, V.; Albin, V.; Ringuedé, A.; Cassir, M. Theoretical Predictions vs. Experimental Measurements of the Electrical Conductivity of Molten Li_2CO_3-K_2CO_3 Modified by Additives. *Int. J. Hydrog. Energy* **2012**, *37*, 19357–19364. [CrossRef]
50. Ward, A.T.T.; Janz, G.J.J. Molten Carbonate Electrolytes: Electrical Conductance, Density and Surface Tension of Binary and Ternary Mixtures. *Electrochim. Acta* **1965**, *10*, 849–857. [CrossRef]
51. Volkova, L.F. Phase Diagram of K_2CO_3-Na_2CO_3-Li_2CO_3. *Izvest. Sib. Oldel. Akad. Nauk SSSR* **1958**, *7*, 33–35.
52. Huang, J.; Xie, F.; Wang, C.; Mao, Z. Development of Solid Oxide Fuel Cell Materials for Intermediate-to-Low Temperature Operation. *Int. J. Hydrog. Energy* **2012**, *37*, 877–883. [CrossRef]

53. Zhu, B.; Yang, X.T.; Xu, J.; Zhu, Z.G.; Ji, S.J.; Sun, M.T.; Sun, J.C. Innovative Low Temperature SOFCs and Advanced Materials. *J. Power Sources* **2003**, *118*, 47–53. [CrossRef]
54. Schober, T.; Ringel, H. Proton Conducting Ceramics: Recent Advances. *Ionics* **2004**, *10*, 391–395. [CrossRef]
55. Kreuer, K.D.; Adams, S.; Münch, W.; Fuchs, A.; Klock, U.; Maier, J. Proton Conducting Alkaline Earth Zirconates and Titanates for High Drain Electrochemical Applications. *Solid State Ion.* **2001**, *145*, 295–306. [CrossRef]
56. Pergolesi, D.; Fabbri, E.; D'Epifanio, A.; Di Bartolomeo, E.; Tebano, A.; Sanna, S.; Licoccia, S.; Balestrino, G.; Traversa, E. High Proton Conduction in Grain-Boundary-Free Yttrium-Doped Barium Zirconate Films Grown by Pulsed Laser Deposition. *Nat. Mater.* **2010**, *9*, 846–852. [CrossRef]
57. Xiong, X.; Lei, X.; Zhang, C.; Wang, J.; Huang, K. Synergetic Proton Conduction in $BaZr_{0.8}Y_{0.2}O_3$-Carbonate Composite Electrolyte for Intermediateerature Solid Oxide Fuel Cells. *Solid State Ion.* **2015**, *279*, 66–71. [CrossRef]
58. Chen, C.; Tran, T.; Olivares, R.; Wright, S.; Sun, S. Coupled Experimental Study and Thermodynamic Modeling of Melting Point and Thermal Stability of Li_2CO_3-Na_2CO_3-K_2CO_3 Based Salts. *J. Sol. Energy Eng.* **2014**, *136*, 031017. [CrossRef]
59. Olivares, R.I.; Chen, C.; Wright, S. The Thermal Stability of Molten Lithium–Sodium–Potassium Carbonate and the Influence of Additives on the Melting Point. *J. Sol. Energy Eng.* **2012**, *134*, 041002. [CrossRef]
60. Bros, J.; Gaune-Escard, M. Estimation de l'enthalpie de Fusion de Mélanges Eutectiques de Sels Fondus Utilisables Pour Le Stockage Thermique de l'énergie. *Rev. Phys. Appl.* **1979**, *14*, 107–112. [CrossRef]
61. Zhu, B.; Albinsson, I.; Mellander, B. Intermediate Temperature Fuel Cells Using Alkaline and Alkaline Earth Fluoride-Based Electrolytes. *Solid State Ion.* **2000**, *135*, 1–10. [CrossRef]
62. Zhu, B. Proton and Oxygen Ion Conduction in Nonoxide Ceramics. *Mater. Res. Bull.* **2000**, *35*, 47–52. [CrossRef]
63. Kim, J.T.; Lee, T.H.; Park, K.Y.; Seo, Y.; Kim, K.B.; Song, S.J.; Park, B.; Park, J.Y. Electrochemical Properties of Dual Phase Neodymium-Doped Ceria Alkali Carbonate Composite Electrolytes in Intermediate Temperature. *J. Power Sources* **2015**, *275*, 563–572. [CrossRef]
64. Rondão, A.I.B.; Patrício, S.G.; Figueiredo, F.M.L.; Marques, F.M.B. Role of Gas-Phase Composition on the Performance of Ceria-Based Composite Electrolytes. *Int. J. Hydrog. Energy* **2013**, *38*, 5497–5506. [CrossRef]
65. Lei, X.; Qin, C.; Huang, K. Energetics of Proton Transfer in Alkali Carbonates: A First Principles Calculation. *RSC Adv.* **2015**, *5*, 56205–56209. [CrossRef]
66. Hansen, H.A.; Wolverton, C. Kinetics and Thermodynamics of H_2O Dissociation on Reduced CeO_2(111). *J. Phys. Chem. C* **2014**, *118*, 27402–27414. [CrossRef]
67. Claes, P.; Moyaux, D.; Peeters, D. Solubility and Solvation of Carbon Dioxide in the Molten $Li_2CO_3/Na_2CO_3/K_2CO_3$ (43.5:31.5:25.0 Mol-%) Eutectic Mixture at 973 K. Part I. Experimental Part. *Eur. J. Inorg. Chem.* **1999**, *1999*, 583–588. [CrossRef]
68. Peeters, D.; Moyaux, D.; Claes, P. Solubility and Solvation of Carbon Dioxide in the Molten II. Theoretical Part. *Eur. J. Inorg. Chem.* **1999**, *3*, 589–592. [CrossRef]
69. Zeller, K.P.; Schuler, P.; Haiss, P. The Hidden Equilibrium in Aqueous Sodium Carbonate Solutions—Evidence for the Formation of the Dicarbonate Anion. *Eur. J. Inorg. Chem.* **2005**, 168–172. [CrossRef]
70. Meskine, H.; Gürbüz, E.; Albin, V.; Meléndez-Ceballos, A.; Cassir, M.; Ringuedé, A.; Lair, V. CO_2 Electrolysis in a Reversible Molten Carbonate Fuel Cell: Online Chromatographic Detection of CO. *Int. J. Hydrog. Energy* **2021**, *46*, 14913–14921. [CrossRef]
71. Wang, W.; Wang, S.; Ma, X.; Gong, J. Recent Advances in Catalytic Hydrogenation of Carbon Dioxide. *Chem. Soc. Rev.* **2011**, *40*, 3703–3727. [CrossRef]
72. Huang, J.; Mao, Z.; Yang, L.; Peng, R. SDC-Carbonate Composite Electrolytes for Low-Temperature SOFCs. *Electrochem. Solid-State Lett.* **2005**, *8*, A437. [CrossRef]